NUMERICAL ANALYSIS OF THE HYDRODYNAMIC BEHAVIOR OF LOCK NAVIGATION FILLING AND EMPTYING SYSTEMS

Marcelo Dalla Corte, marcelodallacorte@gmail.com
Rejane de Cesaro Oliveski, decesaroo@gmail.com
UNISINOS – Universidade do Vale do Rio dos Sinos. São Leopoldo – RS - Brazil

Marcelo Giulian Marques, mmarques@iph.ufrgs.br
Paulo Kroeff de Souza, pksouza@iph.ufrgs.br
UFRGS – Universidade Federal do Rio Grande do Sul. Porto Alegre – RS - Brazil

Abstract: Reverse Tainter gates are often used as flow control systems for filling and emptying high lift navigation locks. Aiming at better understanding the outflow dynamics of this device type, research that seeks to associate two types of analysis - numerical and experimental – is being done to identify the flow characteristics and enable the development of solutions that avoid damage to the structure, since they are subject to adverse hydraulic phenomena (extreme efforts, cavitation, etc.). The comparison between the numerical and experimental pressure results shows that the numerical model reproduces with good approximation the flow through the gate.

Keywords: navigation locks, reverse Tainter gate, numerical simulation, CFX.

1. INTRODUCTION

Reverse Tainter gates are often used as flow control system for filling and emptying high lift navigation locks. In this kind of system, several hydraulic phenomena that are nocive for the structure might occur, such as gate vibration; intermittent efforts in the movement device; expansion of efforts related to downpull and uplift phenomena (phenomena that refer respectively to the downthrust and upthrust forces) and cavitation. Furthermore oscillations in the lock chamber water level might occur, provoking excessive efforts in the ship mooring or even collisions between the vessels and the chamber structure. These oscillations depend on the valve operation law that controls the filling and emptying of the chamber and on the asymmetries in the chamber distribution system. Although this kind of problem could be reduced by increasing the valve operation time, this might have adverse economic impacts. Therefore the understanding of the characteristics of this kind of flow is crucial to improve the project and identify critical operating conditions still in the early stages of the project.

This paper aims at carrying out a numerical analysis of the flow through the reverse Tainter gate. The obtained results will be compared with the results obtained in the experimental tests.

2. METHODOLOGY

2.1. Experimental structure

The experimental study of the hydrodynamic behavior characteristics downstream of the gate was developed in a test bench as shown in Fig. 1. This bench enables permanent flow control in different operating and gate opening conditions. In the main conduit downstream of the gate, pressure test connections were defined at the roof and bottom to allow measurements with piezometers and transducers. The bench conduit has a square section of 0.25 meter on the side and is 1.7 meter long upstream and 4 meter long downstream. The chamber is 0.4 meter long and 0.75 meter high. The gate radius of curvature is 0.38 meter and allows opening control from 0% to 100%. The surge chamber diameter is 0.1 meter and 4 meter high. The flow is monitored by an electromagnetic flow meter, located at 4.2m upstream of the gate.

2.2. Numerical model

The numerical simulation of the flow was carried out using the commercial software ANSYS CFX-11. Although the same dimensions as of the experimental apparatus were maintained, the geometric model was simplified (the gate axes and support arms were disregarded). The symmetry condition was also considered in the direction of the bench width. In this way, the numerical model corresponds to half of the physical model. The spatial mesh is hexaedrical and was used the multi-block methodology. Fig. 2 illustrates a detail of the computational mesh in the gate region. In this figure it is possible to observe a high refinement degree in all physical walls of the object. The mesh used has approximately 662,000 volumes.
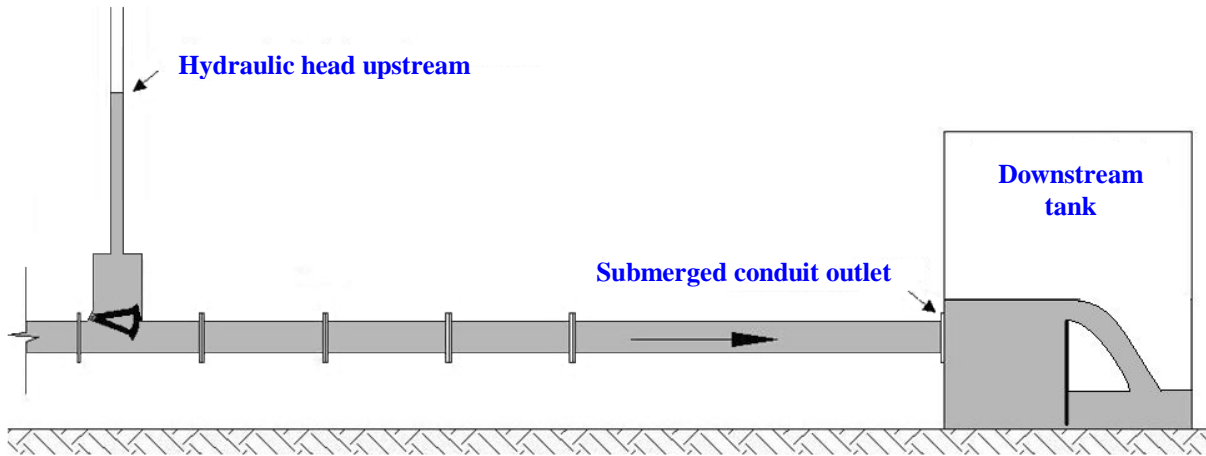
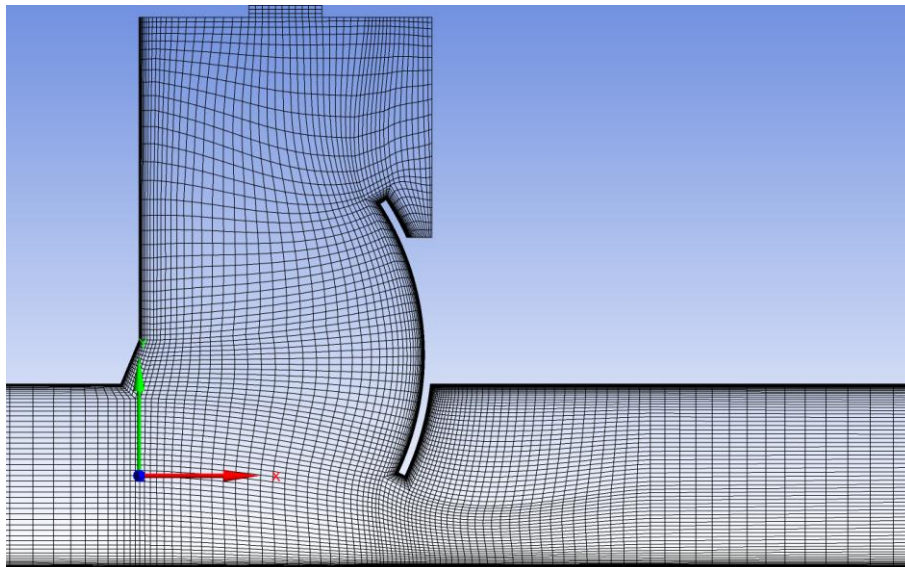Figure 1 – Scheme of the experimental bench.

Figure 2 – Computational mesh.

The numerical model used is tridimensional, homogeneous and composed of mass conservation (Eq. 1) and momentum (Eq. 2) equations.

$$\frac{\partial U_i}{\partial x_i} = 0 \tag{1}$$

$$\rho \left(\frac{\partial U_i}{\partial t} + U_j \frac{\partial U_i}{\partial x_j} \right) = -\frac{\partial p}{\partial x_i} + \mu \frac{\partial}{\partial x_j} \left(\frac{\partial U_i}{\partial x_j} + \frac{\partial U_j}{\partial x_i} \right) + F_{U_i} \tag{2}$$

where ρ is the density, μ the dynamic viscosity, p the pressure, t the time and F_{U_i} the source term.

For its simplicity and robustness, the turbulence model used was the k-ε (Eq. 3 and 4).

$$\rho \left(\frac{\partial \kappa}{\partial t} + \overline{U}_j \frac{\partial \kappa}{\partial x_j} \right) = \frac{\partial}{\partial x_j} \left(\Gamma_\kappa \frac{\partial \kappa}{\partial x_j} \right) + P_\kappa - \rho \varepsilon \tag{3}$$

$$\rho \left(\frac{\partial \varepsilon}{\partial t} + \overline{U}_j \frac{\partial \varepsilon}{\partial x_j} \right) = \frac{\partial}{\partial x_j} \left(\Gamma_\varepsilon \frac{\partial \varepsilon}{\partial x_j} \right) + C_{1\varepsilon} \frac{\varepsilon}{\kappa} P_\kappa - C_{2\varepsilon} \frac{\varepsilon^2}{\kappa} \tag{4}$$

where P_κ is the production of turbulence kinetic energy, Γ_κ the diffusion coefficient in the κ equation, Γ_ε the diffusion coefficient in the ε equation and μ_t the turbulent dynamic viscosity. These terms are obtained respectively by following equations:

$$P_\kappa = \mu_t \left(\frac{\partial \overline{U}_i}{\partial x_j} + \frac{\partial \overline{U}_j}{\partial x_i} \right) \frac{\partial \overline{U}_i}{\partial x_j} \tag{5}$$

$$\Gamma_\kappa = \mu + \frac{\mu_t}{\sigma_\kappa} \tag{6}$$

$$\Gamma_\varepsilon = \mu + \frac{\mu_t}{\sigma_\varepsilon} \tag{7}$$

$$\mu_t = C_\mu \rho \frac{\kappa^2}{\varepsilon} . \tag{8}$$

These equations, as well as the mass conservation and momentum equations, can be numerically solved, since appropriate values are used for the five constants, $C_{1\varepsilon}$, $C_{2\varepsilon}$, C_μ, σ_ε (turbulent Prandtl number in ε equation) and σ_κ (turbulent Prandtl number in the κ equation) present in equations (3) and (4). The values for these constants are:

$$C_{1\varepsilon} = 1.44 \quad C_{2\varepsilon} = 1.92 \quad \sigma_\varepsilon = 1.3 \quad \sigma_\kappa = 1.0 \quad e \quad C_\mu = 0.09 . \tag{9}$$

Boundary Conditions

- inlet: developed profiles of velocity, turbulent kinetic energy and dissipation, obtained from a preliminary simulation of a discharge in a 50 meter square tube of constant section;
- outlet: an expression for pressure linear variation was used as a function of the height, based on the experimental pressure values;
- walls: a non-slip condition was applied, except in the chamber walls, where the free slip condition was applied to simplify the model.
- chamber opening: static pressure equal to 0 Pa.

Initial Conditions

In all studied cases it was necessary to carry out a preliminary simulation (with the same mesh and boundary conditions) using "Local Timescale Factor" in time step, with a factor equal 5. With this option, the software determines a time step for each mesh cell and then multiplies it by the specified factor. A factor with a lower order of magnitude was also specified for the volumetric fraction equation to avoid instabilities in the water-air interface height, since the initial velocity field is highly instable. Then a second simulation was carried out using as initial condition the first simulation result, although now applying a time step type "physical time step" of 0.005 s in all domain and for all equations. The number of iterations was specified at 1000 and the resolution scheme applied was the "High Resolution".

As initial condition for the preliminary simulation, the mean flow velocity at the inlet section was applied in all domain. This value is applied in the direction perpendicular to the inlet and outlet section (direction X), whereby null velocities were applied in the remaining directions. The initial pressure condition is uniform and approximately 500 Pa above the maximum outlet pressure of each case. The water level height is specified according to the pressure obtained in the physical model at point 01MB, located at the conduit bottom in the chamber inlet. Initial values were not specified for the remaining variables, so that the software determines automatically their initial field. This set of initial conditions proved to be more robust and stable, avoiding recirculation at the domain outlet and sudden interface fluctuation, thus achieving good convergence without instabilities or errors.

3. RESULTS

Experimental tests were developed for valve openings of 10 to 100%. The volumetric flow varying from 28 to 180 l/s. In order to facilitate the presentation and analysis of the results, each case study is represented by a code which indicates the gate opening condition and the volumetric flow, as shown in Tab. 1.

Table 1 – Case studies in the present paper.

OPENING [%]	FLOW [l/s]	CODE
10	28	A10Q28
30	40	A30Q40
30	90	A30Q90
30	180	A30Q180
50	40	A50Q40
50	90	A50Q90
50	180	A50Q180
60	90	A60Q90
60	180	A60Q180
70	90	A70Q90
70	180	A70Q180
80	90	A80Q90
80	180	A80Q180
100	90	A100Q90
100	180	A10Q180

In Figs. 3-6 some flow characteristics are presented for the case A50Q180. All simulated cases present similar qualitative behavior. Fig. 3 shows the pressure field in the central domain plan (model symmetry plan). In this figure it is possible to observe the pressure drop just upstream of the valve and the beginning of recovery.

Figure 4 shows a detail of the pressure field in the region of the gate lower edge. The minimum pressures for the conduit bottom and roof are respectively -8 kPa and -10 kPa, and the pressures at the gate edge are -30 kPa. This indicates that this region is a critical point for flow cavitation.

Figure 5 shows the turbulent kinetic energy field in the central domain plan. Figure 6 shows the streamlines also in the central domain plan. This figure displays the recirculation regions upstream and downstream of the gate.
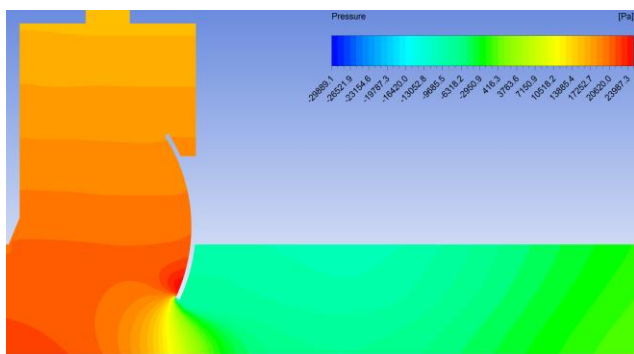
Figure 2 – Pressure field.
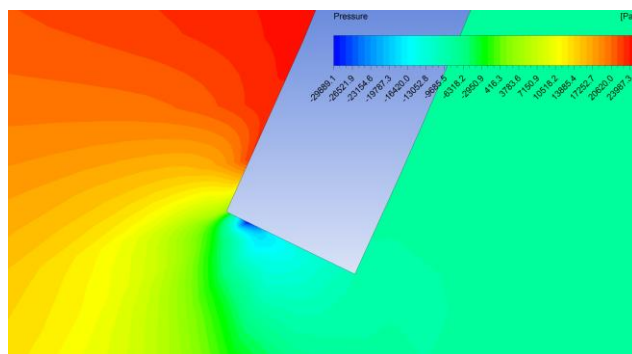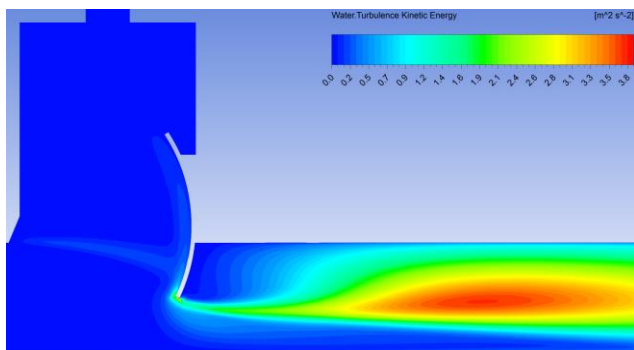

Figure 4 – Detail of the pressure field.

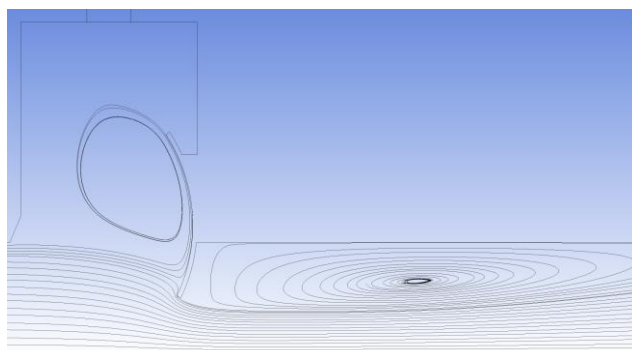Figure 5 – Turbulent kinetic energy field.

Figure 6 – Streamlines.

Figures 7-9 show the experimental mean pressure values and the pressure values estimated by the numerical model at the conduit bottom respectively for cases A70Q90, A50Q90 and A30Q90. Figures 10 and 11 show the pressure values at the conduit bottom for cases A50Q40 and A50Q180. These figures also display the standard deviation bar of the experimental data for the pressure test connections by transducers. The experimental points which do not present the standard deviation bar are points of pressure test connections by piezometers.

The analysis of these figures shows that the numerical model pressure profile follows with good agreement the experimental profile. The difference between the numerical values and the experimental values is close to the experimental standard deviation. It is also possible to observe that the difference is higher in the pressure recovery region and lower in the regions just downstream of the valve and close to the conduit outlet. It was also observed that the experimental standard deviation increases as the gate opening decreases. The experimental standard deviation also increases as the flow increases. In the case with lower flow rate (A50Q40), it could also be observed that the mean pressure values do not follow a well defined pattern as in the case with a higher flow rate (A50Q180).
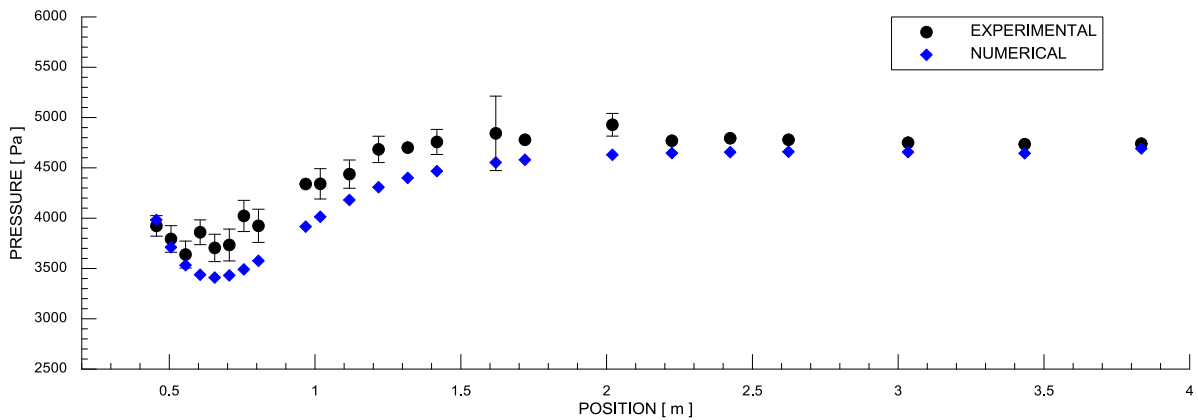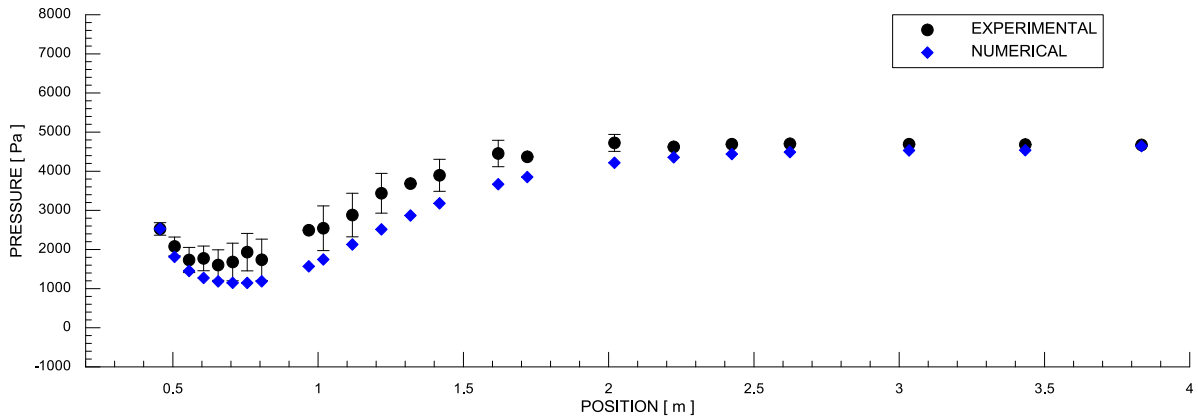

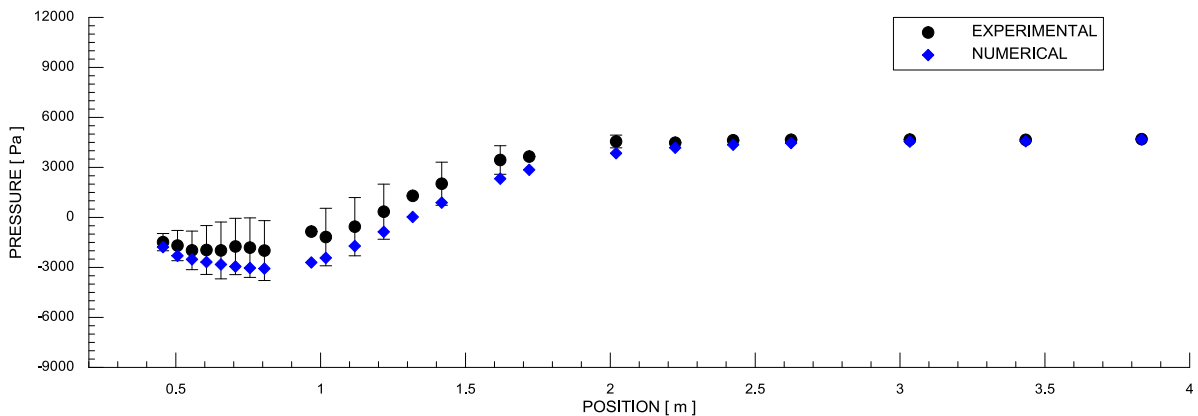Figure 7 – A70Q90 Bottom.

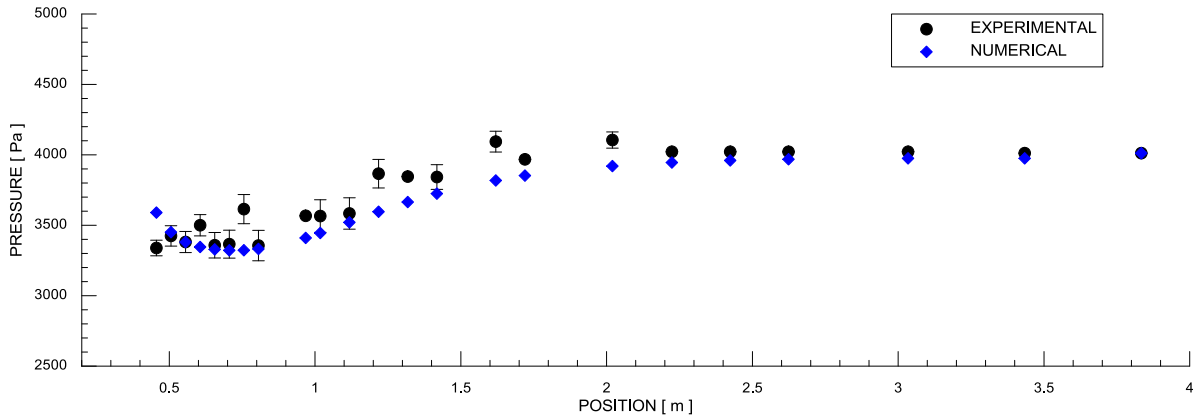Figure 8 – A50Q90 Bottom.

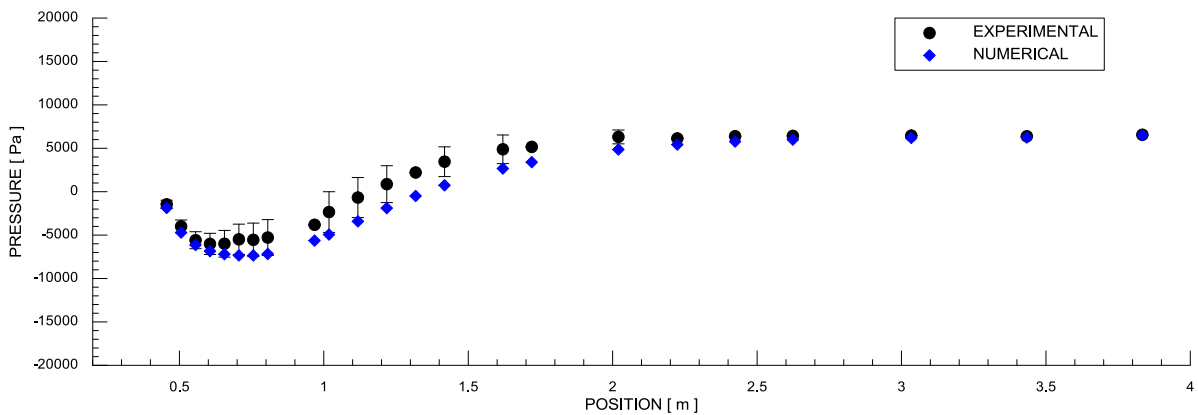Figure 9 – A30Q90 Bottom.

Figure 10 – A50Q40 Bottom.

Figure 11 – A50Q180 Bottom.

Figures 12-16 display graphically the experimental standard deviation of the data obtained in the tests with the physical model and the difference between the experimental mean pressure values and the values estimated by the numerical model at the conduit bottom downstream of the gate for the operating conditions shown in figures 7-11. These figures demonstrate more clearly that the experimental standard deviation and the numerical-experimental difference increase as the flow increases and the gate opening decreases. In case A50Q40, the standard deviation and the numerical-experimental difference have amplitudes of the same order of magnitude, except in some points. In case A70Q90, the numerical-experimental difference is approximately twice the experimental deviation in some points. In case A50Q90, the experimental standard deviation and the numerical-experimental difference are again of approximately the same order of magnitude and the numerical-experimental difference is slightly higher in some points. In case A30Q90, the numerical-experimental difference becomes lower than the experimental standard deviation, whereby at some points it is approximately half of the standard deviation value.
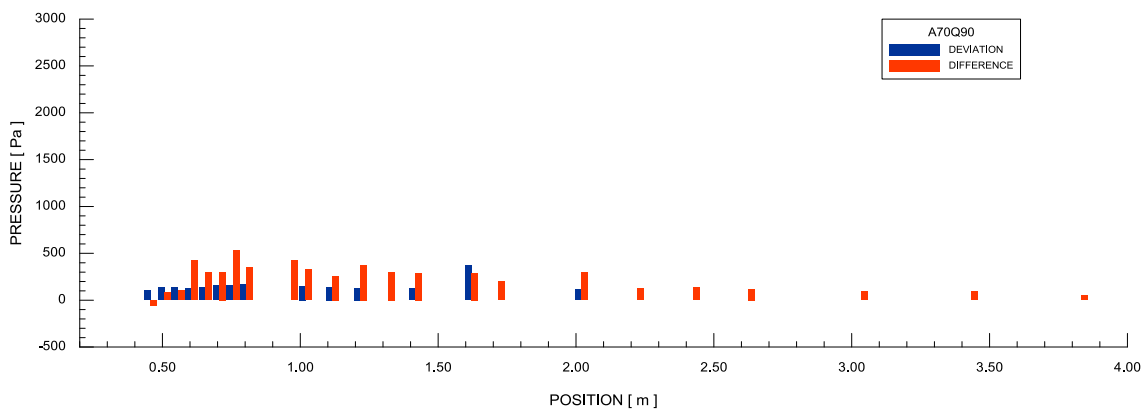

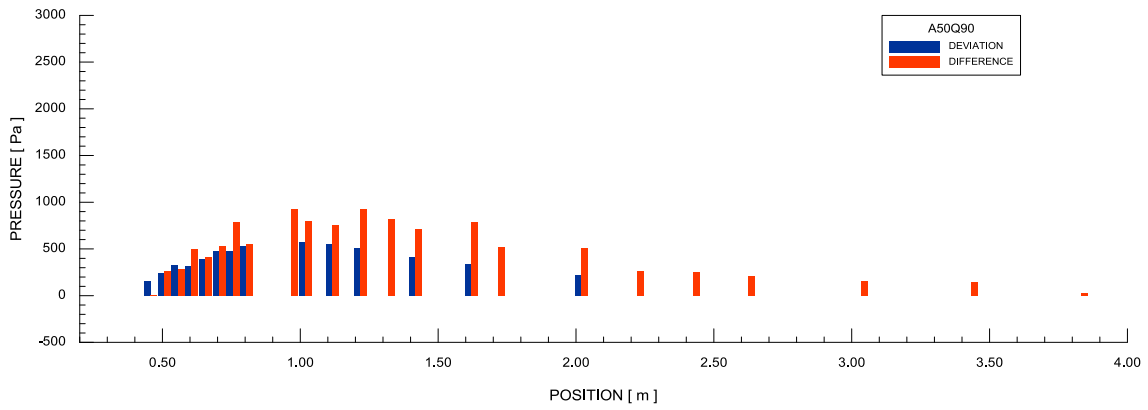Figure 12 – A70Q90 Bottom difference.
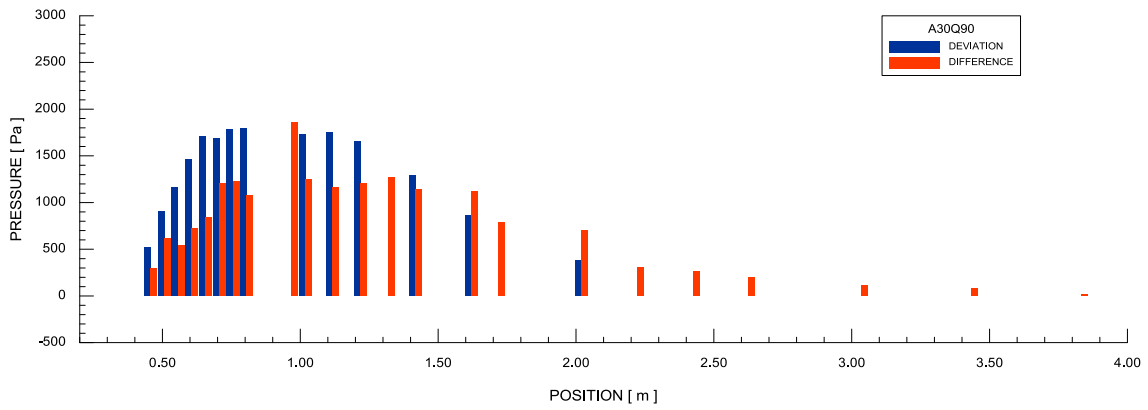
Figure 13 – A50Q90 Bottom difference.
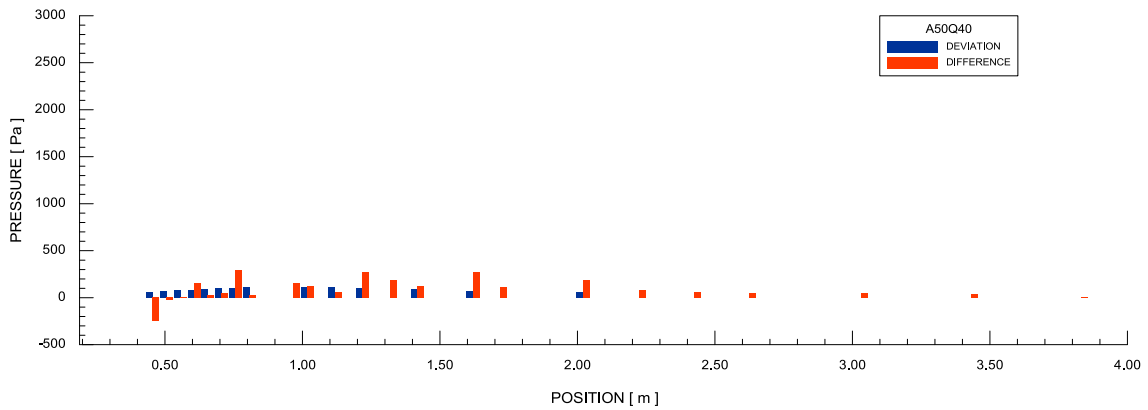

Figure 14 – A30Q90 Bottom difference.

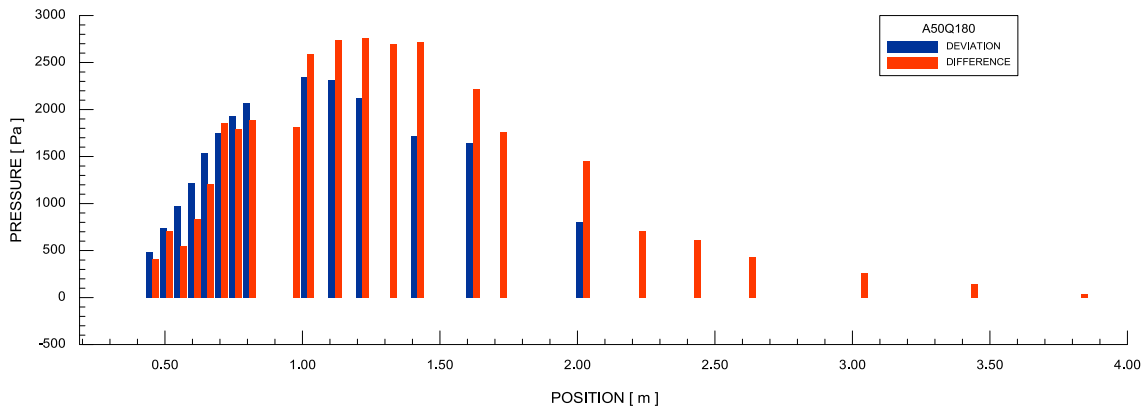
Figure 15 – A50Q40 Bottom difference.

Figure 16 – A50Q180 Bottom difference.

It can also be seen that in all cases both the standard deviation as the numerical-experimental difference also vary with the position along the conduit. Just downstream of the gate there is a sudden increase which remains in this range until the middle conduit region and then decreases towards the conduit outlet. The standard deviation and the numerical-experimental difference at the conduit roof present a similar behavior, slightly diverging in the region immediately downstream of the gate and displaying a slower decrease towards the conduit outlet.

Fig. 17 shows the results obtained for the head loss coefficient (k) in the gate for the operating conditions described. The head loss coefficient values are compared to the reference values from the "HYDRAULIC DESIGN OF LOCK CULVERT VALVES". It is possible to observe that the values obtained with the numerical model show excellent agreement with the reference experimental values.
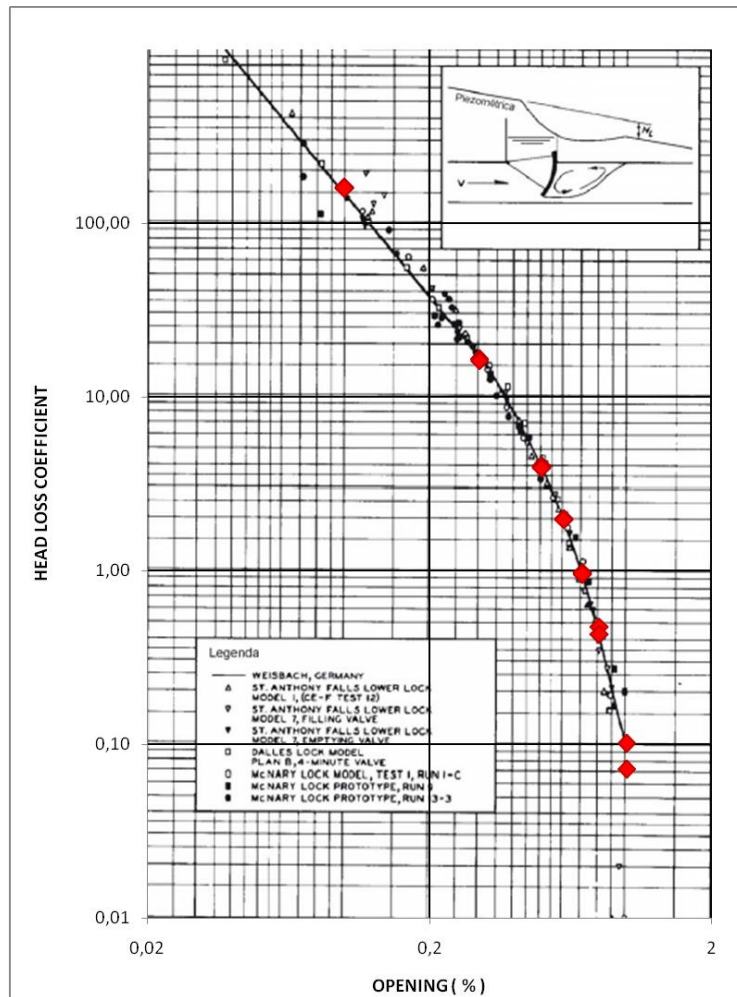

Figure 17 – Head loss coefficient.

4. CONCLUSIONS

The obtained results indicate that the numerical model reproduces with good agreement the experimental results. In all simulated cases, the pressure profile estimated by the numerical model follows the experimental profile. The difference between the pressure values obtained in the numerical model and the physical model values is close to the experimental data standard deviation. Both the standard deviation and the numerical-experimental difference increase as the flow increases. The difference in the pressure values also increases as the gate opening decreases. The difference is higher at the vena contracta region and decreases towards the conduit outlet. The pressure at the lower gate edge presented a significantly lower value than the values obtained downstream of the gate, which indicates that this region is a very critical point for the occurrence of cavitation.

Despite the differences observed in the local pressure values, the head loss coefficient for the gate, which is an important project parameter, showed excellent agreement with the reference values of the literature.

At last it is necessary to continue the study with other cases of different openings and flows in order to further analyze the behavior of the results predicted by the numerical model.

5. ACKNOWLEDGEMENTS

6. REFERENCES

Santos, S.R., 1990, "Efeito de escala no regime de escoamento em eclusas. Previsão do protótipo". In Anais do XIV Congresso Latinoamericano de Hidráulica. Montevideo, Uruguai.

USACE, 1975, United States Army Corps Of Engineers, "Hydraulic design of lock culverts". EM 1110-2-1610. Available at: <http://www.usace.army.mil/publications /eng-manuals/em1110-2-1610/entire.pdf>. Access on: 8th August 2006.

CFX-11.0, User Manual

7. RESPONSIBILITY NOTICE

The authors are the only responsible for the printed material included in this paper.